Electrodermal Mapping of Sympathetic Activation Following Sleep Arousal Onset

Tugce Canbaz Gumussu, *Student Member, IEEE*, Hugo F. Posada-Quintero, *Senior Member, IEEE*, Youngsun Kong, *Member, IEEE*, Camila Jimenez Wong, *Student Member, IEEE*, Ki H. Chon, *Fellow, IEEE*, and Walter Karlen, *Senior Member, IEEE*

***Abstract*— Sleep arousals trigger rapid autonomic shifts, yet their specific sympathetic signatures remain poorly characterized due to the mixed sympathetic-parasympathetic nature of traditional cardiovascular markers. Electrodermal activity (EDA), driven exclusively by sympathetic sudomotor pathways, offers a more direct opportunity to characterize arousal-related autonomic responses during sleep. This study quantifies the evolution of EDA-based features associated with arousal events in 100 adults using polysomnography and high-resolution EDA recordings. We implemented a time-varying frequency decomposition framework to isolate sleep-specific sympathetic components, extracting statistical and peak-based features from arousal segments and matched stable-sleep controls. Compared to controls, arousal segments exhibited robust sympathetic modulation in EDA persisting 40 seconds post-arousal. While long arousals produced robust responses, short arousals showed negligible sudomotor responses. REM and NREM sleep showed consistent feature trajectories, with greater variability during REM. The observed activation is primarily driven by clustered sympathetic bursts and amplitude enhancement rather than shifts in peak frequency. These findings establish EDA as a highly sensitive marker of sleep-related autonomic activation and provide a quantitative baseline for characterizing sympathetic responses to sleep arousals.**

***Index Terms*— Autonomic nervous system, electrodermal activity, galvanic skin response, sleep arousal, sympathetic nervous system.**

I. Introduction

SLEEP arousals are characterized by short altered brain states and often, evoked transient autonomic activations [1]. Prior work attributes these autonomic responses largely to sympathetic nervous system (SNS) activity based on cardiac markers such as heart rate [2] and heart rate variability [3]. Yet, these cardiac measures reflect the combined influence of both sympathetic and parasympathetic branches of the autonomic nervous system, providing an indirect and often ambiguous view of SNS response. This ambiguity hinders our ability to characterize how sleep arousals engage the sympathetic system. A more direct measure of sympathetic responses could help overcome this constraint.

This work was supported by Financial Support Programmes for Female Researchers, Office for Gender Equality, Ulm University.

Tugce Canbaz Gumussu and Walter Karlen are with the Institute of Biomedical Engineering, Ulm University, Ulm, Germany (e-mail: tugce.canbaz@uni-ulm.de).

Youngsun Kong, Camila Jimenez Wong, Hugo F. Posada-Quintero and Ki H. Chon are with Department of Biomedical Engineering, University of Connecticut, Storrs, CT, United States.

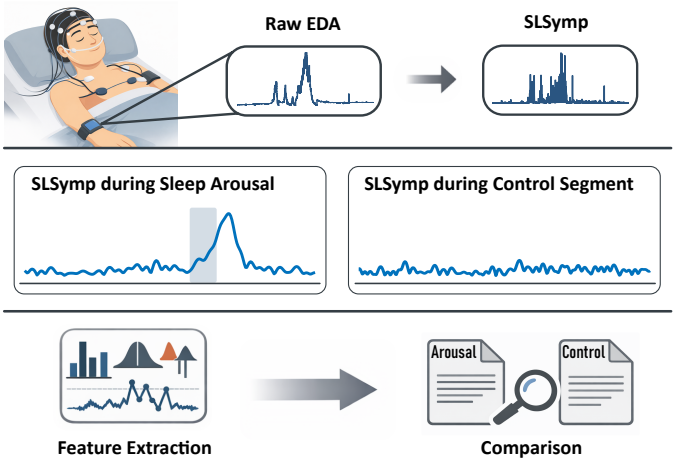

Fig. 1. Analysis of sympathetic responses during sleep arousals. We extracted a sleep-specific sympathetic component (SLSymp) from wrist electrodermal activity (EDA), segmented signals into arousal and control segments, and quantified feature changes to compare arousal-related with control autonomic dynamics. The blue shaded region indicates the sleep arousal window.

Electrodermal activity (EDA) offers a direct measure of sympathetic responses. The eccrine sweat glands in the skin are exclusively innervated by sympathetic nerve fibers [4], and their activation increases skin moisture, thereby enhancing electrical conductivity. This change can be measured non-invasively at the skin surface, providing a specific peripheral marker of sympathetic sudomotor responses. Importantly, unlike cardiac measures, EDA reflects sympathetic output without parasympathetic influence [5], making it an unambiguous window into sympathetic engagement during sleep arousals.

While researchers have widely used EDA to study physiological arousals during wakefulness [6], its relevance to sleep has received growing attention. Prior works have characterized EDA patterns across sleep stages [7] and in deep sleep [8], and have explored its utility for sleep staging [9] and sleep–wake classification [10]. However, despite the role of sleep arousals as key modulators of autonomic state, no prior work has characterized EDA dynamics during arousal events or compared EDA dynamics with stable, non-arousal sleep periods.

In this work, we investigate sympathetic responses during sleep arousals using EDA and characterize how EDA-derived features evolve from before to well after arousal onset (Figure 1). Our main contributions are as follows:

- We introduce a frequency-domain characterization of EDA during sleep to identify the spectral components most dominant during stable sleep and arousals.
- We provide the first systematic, segment-wise analysis of EDA dynamics across arousal events, revealing arousal-specific sympathetic responses distinct from background sleep variability.
- We present the influence of arousal duration and sleep stage on EDA dynamics, highlighting the differences in sympathetic responses across different conditions.

II. Methods

We developed an EDA analysis framework to characterize sympathetic responses associated with sleep arousals. In this framework, we combined time-frequency decomposition with structured signal segmentation to track how sympathetic response evolves before and after arousal onset. By comparing arousal-centered segments with duration-matched control segments from stable sleep, we isolated arousal-specific dynamics from background sleep-related fluctuations. We further assessed how arousal duration and sleep stage influenced these responses. We applied the analysis framework to an open-source dataset with wrist-recorded EDA, obtaining a systematic evaluation of sympathetic activation during sleep arousals.

A. EDA Signal Processing

Sympathetic activity fluctuates dynamically over time and prior work has shown that time-varying analyses of EDA can provide sensitive markers of physiological arousal [11], [12]. To capture these fluctuations during sleep, we used a frequency-selective, time-varying decomposition approach.

We used variable-frequency complex demodulation (VFCDM) [13] to decompose the EDA signal into narrowband oscillatory components, similar to previously proposed frequency-domain characterizations of EDA [11]. We used VFCDM because it provides higher time-frequency resolution and more reliable amplitude estimation than alternative approaches such as wavelet transform [13]. After decomposition, we applied the Hilbert transform to the sum of the reconstructed components to obtain the instantaneous amplitude. Only components within the activity-specific frequency bands were reconstructed.

As the dominant frequency range for sleep-related sympathetic responses has not been firmly established, we first performed a frequency-domain characterization to guide band selection. We analyzed two types of 1-min EDA windows: (1) *reference windows*, drawn from stable sleep without arousals, apneas, or wake epochs; and (2) *arousal-onset windows*, starting at arousal onset but still free of apnea or wake contamination. These windows allowed us to compare baseline spectral content with arousal-associated spectral changes.

TABLE I
Frequency bands (Hz) used for EDA decomposition.

Band 1	Band 2	Band 3	Band 4
0.01–0.045	0.045–0.15	0.15–0.25	0.25–0.45
Band 5	**Band 6**	**Band 7**	**Band 8**
0.45–0.55	0.55–0.70	0.70–0.80	0.80–0.95

We high-pass filtered (fourth-order Butterworth, $0.01\,\mathrm{Hz}$ cutoff) the $4\,\mathrm{Hz}$ EDA to remove baseline drift and its harmonics. For each window, we estimated the power spectral density using Welch's method (60-sample windows, 50% overlap).

We identified dominant frequency bands among eight low-frequency EDA bands (Table I). For each subject, we computed the relative power of each band P_b to obtain the total power such as $P_\mathrm{t} = \sum_{b=1}^{8} P_\mathrm{b}$. Therefore, the percentage power contribution of each band was $(P_\mathrm{b}/P_\mathrm{t}) \times 100$. We sorted the percentage power values in descending order and computed ratios between consecutive slopes to locate the transition from steep to gradual decline. We selected the frequency bands preceding this transition as dominant.

Thereafter, we high-pass filtered the raw EDA signal using a fourth-order Butterworth filter ($0.01\,\mathrm{Hz}$ cutoff) to remove tonic drifts. We then extracted sympathetic tone by applying VFCDM restricted to the selected bands. For this, let $x(t)$ denote the high-pass filtered EDA signal. VFCDM reconstructs the selected components, whose sum we denote as $X'(t)$. We normalize $X'(t)$ by its standard deviation, compute its Hilbert transform and obtain $Y'(t)$. Together, $X'(t)$ and $Y'(t)$ form a complex conjugate pair that defines the analytic signal $Z(t)$ as

$$Z(t) = X'(t) + iY'(t) = a(t)e^{j\theta(t)},$$

where

$$a(t) = \sqrt{X'^2(t) + Y'^2(t)}, \qquad \theta(t) = \arctan\left(\frac{Y'(t)}{X'(t)}\right).$$

We defined the instantaneous amplitude $a(t)$ as SLSymp, denoting its role as a sleep-specific index of sympathetic activation.

B. Segment Extraction

To analyze the dynamics of EDA during sleep arousals, we performed all analyses on the SLSymp signal. For each annotated arousal, we extracted a segment of approximately $80\,\mathrm{s}$, with exact duration depending on the length of the arousal. For every arousal segment, we also generated a corresponding control segment matched in structure and duration from stable sleep without arousals. We divided all arousal and control segments into consecutive $10\,\mathrm{s}$ windows, which served as the units of analysis. The $10\,\mathrm{s}$ window length was chosen because electrodermal responses evolve slowly, and this duration provides sufficient temporal resolution while still capturing meaningful sympathetic activity changes.

Arousal Segments: For each labeled arousal, we extracted a segment beginning $10\,\mathrm{s}$ before arousal onset and extending $60\,\mathrm{s}$ beyond arousal end. Because arousal durations varied, segments exceeded $80\,\mathrm{s}$ whenever the arousal lasted longer than $10\,\mathrm{s}$. For arousals shorter than $10\,\mathrm{s}$, we imposed a

minimum duration of 10 s (i.e., arousal end = onset + 10 s) to ensure a meaningful analysis window.

Each arousal segment was partitioned into consecutive 10 s windows without overlap (Figure 2):

- **W-1:** the 10 s window preceding arousal onset,
- **W0:** the window covering the entire arousal duration (minimum 10 s),
- **W1–W6:** six consecutive 10 s windows following the W0 window.

We included only arousals occurring during sleep. Any segment containing wake epochs within its windows was discarded. Because apneic events substantially influence sympathetic activity [14], [15], we excluded arousals associated with apnea. An arousal was considered apnea-associated if either its W-1 or W0 window overlapped with an apneic event, consistent with the physiological pattern in which apneas commonly terminate with an arousal and resumption of breathing [16].

Control Segments: For each arousal, we randomly selected a matched control segment from stable sleep that was free of arousals, apneas, and wake epochs. Each control segment mirrored its corresponding arousal segment in total duration, number of windows, and window lengths (W-1, W0, and W1–W6). This one-to-one matching allowed direct, window-wise comparisons between arousal-related and stable sleep EDA dynamics while controlling for segment structure and temporal context.

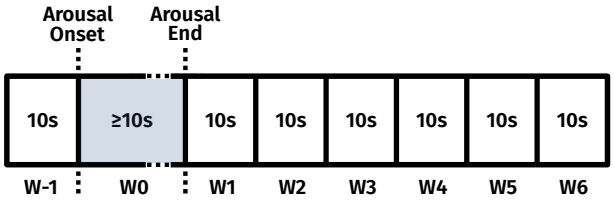

Fig. 2. Windowing of arousal segments. W-1 is the 10 s window before arousal onset. W0 starts with the arousal onset and includes the entire arousal. The minimum duration of W0 window is 10 s. The windows from W1 to W6 are consecutive 10 s windows after W0.

C. Feature Extraction

We computed the following four amplitude-based features for every 10 s window (W-1, W0, W1–W6) in both arousal and matched control segments:

- **Min amplitude:** minimum SLSymp value within the window,
- **Max amplitude:** maximum SLSymp value within the window,
- **Min–max amplitude:** difference between maximum and minimum SLSymp values,
- **Standard deviation (SD):** sample standard deviation of SLSymp values.

In addition to amplitude-based features, we quantified peak dynamics across the ≥ 70 s interval spanning the W0 through W6 windows. Prior work introduced *storm*, defined as repeated EDA peaks occurring within a short time window during sleep [7], [17]. We classified a segment as a storm if it contained a minimum number of peaks within the analysis window. To evaluate whether arousals not only increase the likelihood of peak occurrence but also affect the number of peaks, we examined storms defined by at least two, three, and four peaks. For each subject, we detected storms and computed their proportion relative to the total number of available segments. Because no consensus exists regarding the optimal threshold for defining a peak, we detected storms across multiple peak amplitude thresholds (0.05, 0.1, 0.2, 0.3, and 0.4 µS).

We focused our analysis on SLSymp, which captures the fast components of EDA signals and characterizes sympathetic dynamics. We did not include skin conductance level (SCL) features as SCL reflects slow tonic changes in EDA that can be influenced by many confounding factors, such as hydration level, making it less optimal for our analysis. We also excluded conventional skin conductance response (SCR) features, which quantify rapid transient EDA changes in the time domain (e.g., SCR rate or amplitude). Prior work has shown that time-varying spectral analyses of EDA capture information comparable to these SCR measures [18].

D. Event Analysis

We performed all analyses on z-normalized features except the storms. Normalization was within subjects to account for inter-individual differences in overall SLSymp magnitude across the W-1 to W6 interval and was applied separately to arousal and control segments. For every subject and feature, we first aggregated all available segment values across the entire analysis window (W-1, W0, W1–W6). Let $\{x_1, x_2, \ldots, x_K\}$ denote this aggregated set of values for a given subject. We then computed that subject's normalization parameters mean μ and standard deviation σ. Normalization of each segment value for that subject was using $x^{\text{norm}} = (x - \mu)/\sigma$. This procedure ensured that all feature trajectories were expressed relative to each subject's own baseline distribution while preserving the window-to-window patterns.

After normalization, we first examined arousal and control segments to characterize how SLSymp features evolve from W-1 through the W0 and W1–W6 windows. To do this, we fitted linear mixed-effects models (LMMs) with SLSymp features as the dependent variable, time segment as a fixed effect, and subject as a random intercept, separately for the arousal and control conditions. We then applied analysis of variance (ANOVA) to each model, and when we detected a significant effect ($p<0.5$), we performed pairwise comparisons using estimated marginal means (EMM). We used EMM to test window-to-window temporal changes within each condition after adjusting p-values with the Tukey method. We also compared arousal and control conditions to determine whether arousals induce distinct EDA patterns beyond typical sleep-related variability.

Because arousal duration modulates autonomic responses [19], we evaluated how arousal length influences SLSymp changes. Using the guideline-defined 3s minimum duration [20], we tested thresholds from 3 to 15s in 1s increments. For each threshold, we classified arousals as short ($\leq$ threshold) or long ($>$ threshold). We then fitted an

LMM with the SLSymp feature as the dependent variable, arousal duration group (short vs. long) and time segment (W-1, W0, W1–W6) as fixed effects, and subject as a random intercept. We applied ANOVA to test for main effects and the duration-segment interaction. When the interaction was significant ($p<0.5$), we used EMM for window-to-window comparisons within the arousal duration groups and adjusted p-values with the Tukey method.

Finally, we tested whether the EDA responses to arousal differed across sleep stages. Rapid eye movement (REM) sleep is classically associated with higher sympathetic activity [21], yet prior work has shown that meaningful EDA dynamics also occur during non-REM (NREM) sleep [7]. We assessed stage-specific effects to determine whether arousal-related SLSymp changes reflect general autonomic activation or sleep-stage–dependent mechanisms.

In addition to the amplitude-based feature analysis, we compared the proportion of storms between arousal and control segments across all amplitude thresholds. This threshold-resolved comparison allowed us to evaluate whether differences in storm occurrence remained consistent regardless of the specific peak-detection criterion.

E. Data

We applied our analysis framework on the open-source Dataset for Real-time Sleep Stage Estimation using Multisensor Wearable Technology [22], [23], available on PhysioNet [24]. The dataset contained recordings from 100 participants, including both individuals without sleep disorders and those with sleep-related conditions such as obstructive sleep apnea, excessive daytime sleepiness, or restless leg syndrome. We excluded the recordings with constant EDA channels.

Overnight polysomnography (PSG) recordings had been acquired by the original dataset providers using the Nihon Kohden Polysmith 1004 (version 11) data management system. The PSG setup had included electroencephalography (EEG), electromyography (EMG), electrooculography, electrocardiography, respiratory effort, airflow, and oxygen saturation signals sampled at 200 Hz. During the overnight PSG sessions, participants had worn the Empatica E4 wristband (Empatica Inc., Milano, Italy; software version Summer 2019) on the left wrist, as part of the data acquisition protocol. The wearable signals had included blood volume pulse sampled at 64 Hz, accelerometer at 32 Hz, and temperature and EDA at 4 Hz.

All wearable and PSG signals had been resampled to 100 Hz by the dataset curators to ensure a unified sampling rate across modalities. Wearable and PSG streams had been synchronized by timestamp alignment, as provided in the released dataset. For our analysis, we downsampled the time-aligned EDA signal from 100 Hz to 4 Hz after applying an anti-aliasing filter (fourth-order Butterworth, 2 Hz cutoff).

Sleep stages (Wake, N1, N2, N3) were manually scored in 30 s epochs. The dataset also included technician annotations for apnea events.

F. Arousal Labeling

The sleep arousal labels were not available in the dataset. Therefore, we detected arousals automatically using an open-source algorithm [25] that has been independently validated and shown robust performance across diverse datasets [26]. The algorithm operated on the PSG-derived C4–M1 EEG channel, the chin EMG signal, and the manually labeled sleep stage annotations. Within 3-second sliding windows, the algorithm computed alpha band power and beta band power as features. As an additional feature, EEG signal amplitude changes were also calculated. Candidate arousals were identified when these features exceeded predefined thresholds (alpha power > 0.25, beta power > 0.4, amplitude > 4).

For each candidate, EMG activity within and around the event was evaluated to refine event boundaries and estimate arousal duration. The algorithm then applied exclusion rules derived from the scoring guidelines [20], including the 3 s minimum arousal duration and the requirement of at least 10 s of preceding stable sleep. Events not meeting these criteria were discarded.

TABLE II
DEMOGRAPHIC, CLINICAL, AND DATASET CHARACTERISTICS OF THE STUDY POPULATION. VALUES ARE REPORTED AS MEAN ± SD.

Characteristic	Value	Description
Number of subjects	97	Final cohort size
Female (%)	52 (53.6%)	Sex distribution
Age (years)	56.33 ± 16.59	Age distribution
BMI (kg/m^2)	35.80 ± 23.96	Body–Mass Index
AHI (events/h)	16.60 ± 19.68	Apnea–Hypopnea Index
OAHI (events/h)	16.60 ± 19.68	Obstructive AHI
AI (events/h)	19.29 ± 21.40	Arousal Index
MAD (s)	7.13 ± 3.73	Mean Arousal Duration

G. EDA Signal Quality Analysis

We assessed EDA signal quality using an open-source preprocessing toolbox for ambulatory EDA data [27]. The method evaluated signal quality in consecutive 2-s windows. First, the EDA level was checked to confirm that it was within the physiologically plausible range of 0.05–60 µS. Second, the rate of change was examined; windows exhibiting abrupt changes exceeding $10\,\mu\mathrm{S\,s^{-1}}$ were flagged as invalid, as such rapid fluctuations were typically caused by motion artifacts or sensor instability rather than true physiological responses. Only windows passing both criteria were retained for subsequent analyses. If we could not construct a matched control segment for a given arousal because of poor signal quality or excessive numbers of arousals or apneic events, we excluded the entire recording.

We performed the signal processing with MATLAB R2021b (The MathWorks, Massachusetts, USA). For the statistical analyses, we used R (Version 4.5.1).

III. RESULTS

From the initial cohort of 100 subjects, we excluded one participant (ID 97) due to constant EDA values throughout the entire recording. We also excluded two participants (ID 46 and ID 59) because their unusually high numbers of arousals and apneic events prevented the selection of a sufficient number of

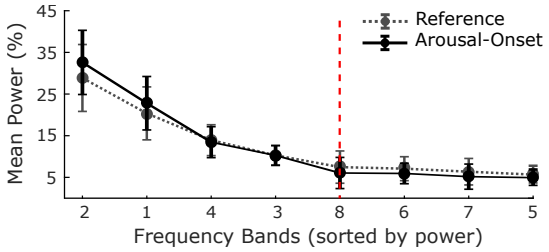

Fig. 3. Mean bandpower contributions with standard error bars across 1-min arousal-onset and reference windows. We sorted bands by mean power in descending order. The red dashed line marks the transition from steep to gradual decline. We defined bands with mean power above this transition as dominant.

TABLE III

EFFECT OF AROUSAL DURATION THRESHOLD ON SHORT AROUSALS. * INDICATES A STATISTICALLY SIGNIFICANT DIFFERENCE RELATIVE TO W1 ($p < 0.05$, TUKEY-ADJUSTED). ALL WINDOW COMPARISONS FOR LONG AROUSALS WERE SIGNIFICANT AT ALL THRESHOLDS.

Threshold (s)	$n_{\textbf{short}}$	**Significant difference relative to W0**		
		W2	**W3**	**W4**
3	65	–	–	–
4	465	–	–	–
5	835	–	–	–
6	1129	–	–	–
7	1338	–	–	–
8	1489	–	–	–
9	1636	–	–	–
10	1744	–	–	–
11	1831	–	–	–
12	1902	*	*	–
13	1971	*	*	*
14	2033	*	*	*
15	2082	*	*	*

matched control segments. Hence, the final dataset included 97 subjects with a mean age 56.33 ± 16.59 (Table II). Across these participants, we detected 3125 arousal events. After removing events overlapping with apnea, wake epochs, or segments containing low-quality EDA, we retained 2175 arousal segments and an equal number of matched control segments. The REM and NREM sleep distribution was balanced across arousal and control segments, with 1894 arousal, 1925 control segments in NREM and 250 arousal, 281 control segments in REM.

The frequency analysis showed that band 8 was the transition from steep to gradual decline for both arousal-onset and reference windows (Figure 3). As bands 1–4 preceded this transition exhibiting higher mean power, we used them for extracting SLSymp. When averaged from $20\,\mathrm{s}$ before to $70\,\mathrm{s}$ after arousal onset across all subjects, the mean SLSymp signal showed a clear post-onset increase, reflecting a characteristic sympathetic activation (Figure 4).

Across all EDA-derived features, arousal segments exhibited approximately threefold larger rise and decay amplitudes than matched control segments, indicating stronger sympathetic activation during arousals (Figure 5). Feature values increased with the arousal onset and remained elevated for up to approximately $40\,\mathrm{s}$ afterward. Window-to-window comparisons further supported this pattern. All features showed significant increases from the W-1 and the W0 windows to W2, W3, and W4 windows, confirming a robust SLSymp response at arousal onset. These sustained increases demonstrated that sympathetic response persisted for several tens of seconds following arousal, rather than returning immediately to baseline.

Because all features showed highly similar temporal patterns across segments (Fig. 5) and there were consistent increases from W-1 to W2–W4 and from W0 to W2–W4, we reported the arousal duration analysis using a representative feature (max amplitude) to avoid redundancy (Table III). This summary captured the similar effects observed across the full feature set. We found that short arousals exhibited no significant change from W-1 to W2–W4 until the duration threshold reached $12\,\mathrm{s}$. The changes for long arousals were significant across all duration thresholds, indicating that autonomic responses increase with arousal length.

When analyzing the features by sleep stage, feature trajectories showed broadly similar temporal patterns in REM and NREM sleep (Figure 6). However, REM sleep showed a remarkable increase in W4, which was not observed in NREM sleep. REM sleep also exhibited greater inter-subject variability, reflected by larger standard error values, consistent with the higher and more heterogeneous sympathetic activity typically observed during this stage.

Across all peak-count criteria used to define storms, arousal segments contained a higher proportion of storm-positive epochs than matched control segments (Figure 7). This finding indicates that EDA storms are more likely to occur in temporal association with arousal events. Notably, the difference between arousal and control segments segments remained stable across thresholds, suggesting that this association does not depend on the specific storm definition.

IV. DISCUSSION

In this study, we showed that sleep arousals are accompanied by marked increases in SLSymp features, with elevated sympathetic response persisting for approximately $40\,\mathrm{s}$ after arousal termination. We systematically characterized the temporal dynamics of electrodermal activity around sleep arousals using a decomposition framework tailored for sleep. By comparing arousal segments with matched control segments, we demonstrated that arousals evoke a clear and sustained sympathetic response beyond the background fluctuations observed during stable sleep. In addition, arousal segments exhibited a higher prevalence of EDA storms than control segments, further supporting the close temporal association between arousals and transient bursts of sympathetic activation.

The amplitude-based feature analysis revealed consistent increases across all metrics immediately after arousal onset. All the examined measures showed significant elevations in the W2 to W4 windows relative to the W-1 and W0 windows. These temporal patterns suggest a characteristic rise-and-decay response, indicating that the effect of arousal-related sympathetic activation persist up to 40s before returning toward baseline. The sustained increases likely reflected both continued sympathetic sudomotor activity after arousal termination and the slow recovery of sweat gland function, where secreted sweat persists before evaporating or being reabsorbed.

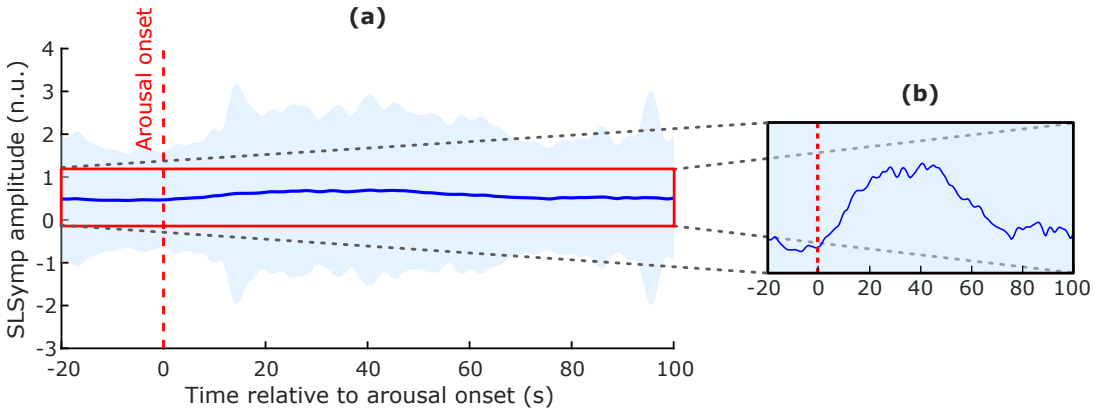

Fig. 4. Temporal dynamics of sympathetic response around sleep arousals. (a) Mean SLSymp amplitude across all arousals and subjects, showing the time course from $20\,\mathrm{s}$ before to $100\,\mathrm{s}$ after arousal onset. The blue shaded region represents the standard error of the mean. The red vertical dashed line at time zero marks arousal onset. (b) A magnified view of the arousal response, highlighting the peak activation occurring approximately $20\,\mathrm{s}$ after arousal onset and the gradual return toward baseline.

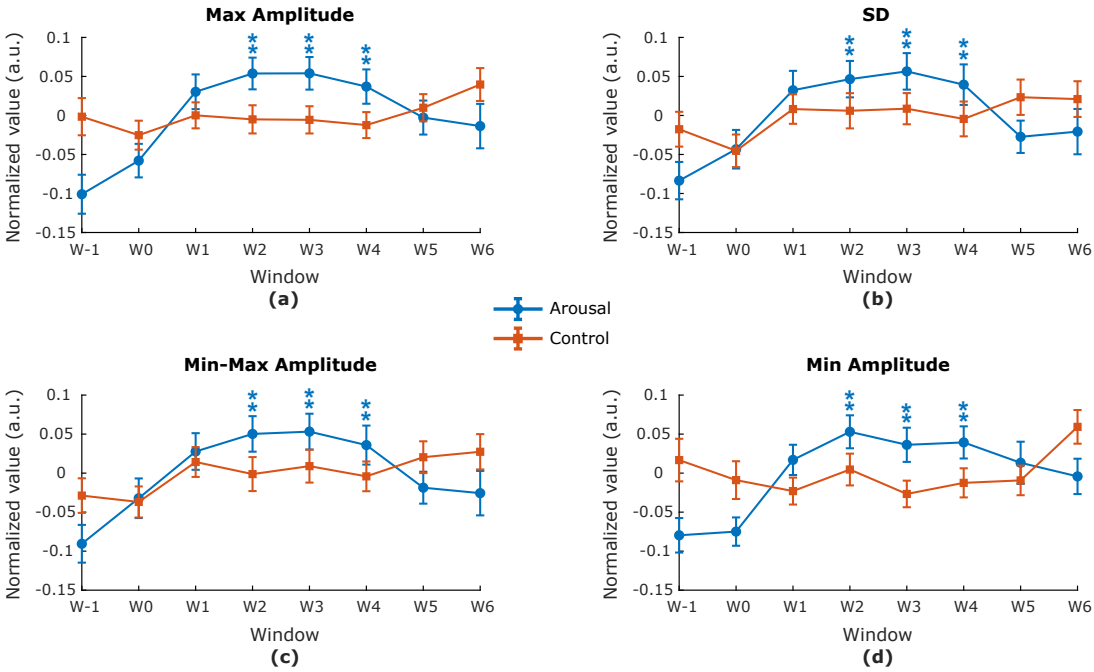

Fig. 5. Normalized trajectories of SLSymp features across arousal and control segments. Each panel shows the mean with standard error bars across all arousal (blue) and matched control (orange) segments for four amplitude-based features: (a) maximum amplitude, (b) standard deviation, (c) min–max amplitude range, and (d) minimum amplitude. Feature values are normalized within subject and plotted across seven consecutive windows (W-1, W0, W1–W6). Across features, arousals are associated with a rise in amplitude-related metrics immediately after onset, followed by a gradual return toward baseline, whereas control segments remain comparatively stable. Upper and lower asterisks mark significant increases ($p < 0.01$) in windows W2–W4 compared with W-1 and W0, respectively.

Arousal duration further modulated amplitude-based feature responses. Although both short and long arousals increased feature amplitudes, only longer events generated consistent statistically significant changes. This does not imply an absence of sympathetic activation during short arousals; rather, the associated responses may be weaker or more transient and hence less consistently captured by EDA-derived features. These findings support prior observations that arousal duration influences the magnitude of the autonomic response [19] and suggest a threshold-like relationship between arousal length and the detectability of sympathetic engagement in EDA.

Feature trajectories were similar between REM and NREM sleep, but REM segments exhibited noticeably higher variability. This larger variance may reflect the intrinsically fluctuating autonomic environment of REM sleep, where sympathetic activity is known to be elevated. It is also important to note that the number of REM segments was substantially smaller than that of NREM, which may have contributed to the increased variability through reduced averaging.

Our analysis showed that arousals markedly increased the likelihood of EDA storms. Prior work demonstrated that storms occur naturally throughout sleep as part of baseline sympathetic activity [7]. We observed this same phenomenon in our data: both arousal and control segments exhibited

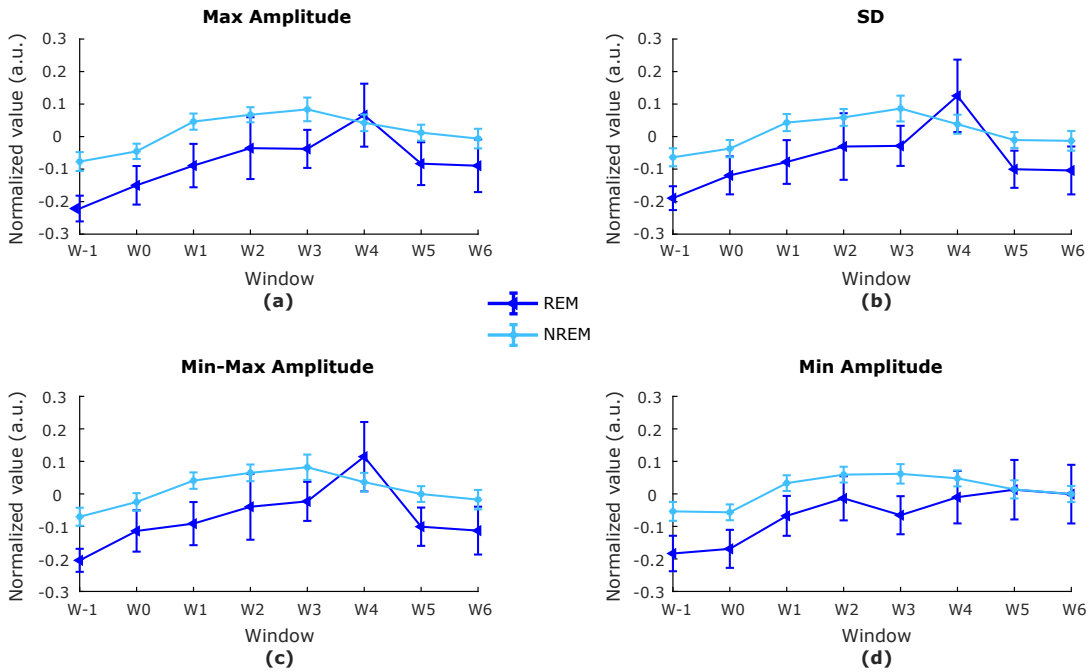

Fig. 6. Normalized SLSymp feature trajectories during arousals for REM and NREM sleep. Each panel shows the mean normalized feature values with standard error bars across seven temporal segments (W-1, W0, W1–W6). Features include (a) maximum amplitude, (b) standard deviation, (c) min–max amplitude, and (d) minimum amplitude. REM (dark blue) and NREM (light blue) segments are shown separately to illustrate stage-specific differences in sympathetic dynamics. Across both sleep stages, arousal onset produces a pronounced rise and gradual decay in amplitude-based features, with REM segments exhibiting greater variability.

storms, confirming that spontaneous peak bursts are an expected component of normal sleep physiology. Our study additionally showed that arousal segments consistently included a higher proportion of storms. Importantly, this increase did not coincide with a higher number of peaks within storms compared to control segments. Thus, arousals appear to elevate the probability that a storm occurs rather than altering the storm structure itself.

When interpreting storm dynamics together with the statistical SLSymp features, a coherent pattern emerges. Arousal onset produced robust increases in statistical, amplitude-based features but did not yield additional peaks within storms. This indicates that the sympathetic response to arousals manifests primarily as enhanced magnitude rather than increased frequency of electrodermal events. One possible physiological explanation is the transient synchronization of sweat gland activity during arousals. Increased sympathetic outflow during arousal may recruit additional glands or enhance temporal coordination, producing larger, more spatially coherent skin conductance responses without requiring additional discrete sympathetic bursts. As a result, peaks that were too small to detect during stable sleep become detectable during arousal, increasing storm likelihood without proportionally increasing peak counts. This represents a shift in the amplitude distribution of sympathetic activity rather than a change in discharge frequency, consistent with arousal-induced reorganization of autonomic output patterns.

While this study provides a robust characterization of arousal-related sympathetic dynamics, several factors define its scope. First, the analysis focused on discrete arousal events without accounting for the potential modulatory effects of concurrent sleep microstructures, such as K-complexes, spindles, or slow-wave activity, which are known to influence autonomic tone [28]. Second, to maintain statistical power across the cohort, sleep stages were analyzed as REM and NREM; future work should explore the finer granularity of N1–N3 substages and the tonic-phasic dichotomy of REM sleep. Additionally, although the automated arousal detection algorithm has been extensively validated, the lack of manual annotations in this specific dataset introduces a potential for minor detection bias. Finally, while this study established a general population baseline, the modulatory role of sex hormones on sudomotor responses was not evaluated and remains a critical area for subsequent investigation.

V. Conclusion

This work provided a comprehensive characterization of sympathetic response during sleep arousals using SLSymp, an EDA decomposition tailored for sleep. By jointly examining amplitude-based SLSymp features, temporal trajectories, arousal-duration effects, and storm dynamics, we showed that arousals elicit a robust, sustained sympathetic response that extends well beyond arousal termination. Our results revealed a consistent rise-and-decay pattern across features, the higher influence of the longer arousals on EDA features, and a marked increase in the likelihood of EDA storms without a corresponding increase in peak count. Together, these findings suggest that arousal-related sympathetic activation manifests primarily through stronger sudomotor responses, likely reflecting transient synchronization of sweat gland activity rather than an

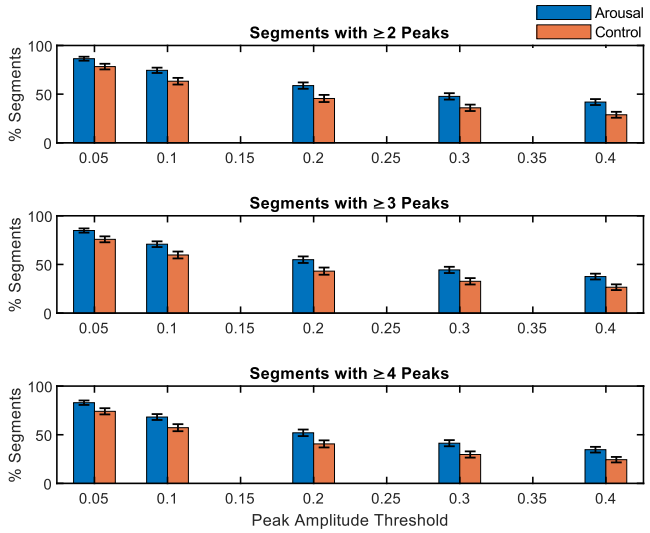

Fig. 7. Percentage of segments containing "storm" across varying peak amplitude thresholds. Each row corresponds to a different minimum peak-count criterion used to define a storm (top: at least two peaks, middle: at least three peaks, and bottom: at least four peaks). For each amplitude threshold on the x-axis, the y-axis shows the percentage of segments classified as storms. Arousal segments (blue) and matched control segments (orange) are displayed side by side to illustrate differences in storm occurrence across conditions.

increase in the number of individual responses. Our findings strengthen the understanding of autonomic processes underlying sleep arousals and underscore the value of EDA as a complementary biomarker for characterizing their physiology.

Acknowledgment

We thank the members of the Chon Lab, the Posada-Quintero Lab, and the Sleeploop consortium for many insightful discussions. We also thank the creators of the open-access dataset used in this work for making the data publicly available.

References

[1] P. Halász et al., "The nature of arousal in sleep," Journal of Sleep Research, vol. 13, no. 1, pp. 1–23, 2004, doi: 10.1111/j.1365-2869.2004.00388.x.

[2] E. Sforza et al., "Heart rate activation during spontaneous arousals from sleep: effect of sleep deprivation," Clinical Neurophysiology, vol. 115, no. 11, pp. 2442–2451, Nov. 2004, doi: 10.1016/j.clinph.2004.06.002.

[3] A. Blasi et al., "Cardiovascular variability after arousal from sleep: time-varying spectral analysis," Journal of Applied Physiology, vol. 95, no. 4, pp. 1394–1404, Oct. 2003, doi: 10.1152/japplphysiol.01095.2002.

[4] C.-Y. Cui and D. Schlessinger, "Eccrine sweat gland development and sweat secretion," Experimental Dermatology, vol. 24, no. 9, pp. 644–650, 2015, doi: 10.1111/exd.12773.

[5] W. Boucsein, Electrodermal Activity. Boston, MA: Springer US, 2012. doi: 10.1007/978-1-4614-1126-0.

[6] R. Sánchez-Reolid et al., "Machine Learning Techniques for Arousal Classification from Electrodermal Activity: A Systematic Review," Sensors, vol. 22, no. 22, p. 8886, Jan. 2022, doi: 10.3390/s22228886.

[7] A. Sano, R. W. Picard, and R. Stickgold, "Quantitative analysis of wrist electrodermal activity during sleep," International Journal of Psychophysiology, vol. 94, no. 3, pp. 382–389, Dec. 2014, doi: 10.1016/j.ijpsycho.2014.09.011.

[8] J. A. Onton, D. Y. Kang, and T. P. Coleman, "Visualization of Whole-Night Sleep EEG From 2-Channel Mobile Recording Device Reveals Distinct Deep Sleep Stages with Differential Electrodermal Activity," Front. Hum. Neurosci., vol. 10, Nov. 2016, doi: 10.3389/fnhum.2016.00605.

[9] A. S. Anusha et al., "Electrodermal activity based autonomic sleep staging using wrist wearable," Biomedical Signal Processing and Control, vol. 75, p. 103562, May 2022, doi: 10.1016/j.bspc.2022.103562.

[10] A. Herlan et al., "Electrodermal activity patterns in sleep stages and their utility for sleep versus wake classification," Journal of Sleep Research, vol. 28, no. 2, p. e12694, 2019, doi: 10.1111/jsr.12694.

[11] H. F. Posada-Quintero et al., "Highly sensitive index of sympathetic activity based on time-frequency spectral analysis of electrodermal activity," American Journal of Physiology-Regulatory, Integrative and Comparative Physiology, vol. 311, no. 3, pp. R582–R591, Sep. 2016, doi: 10.1152/ajpregu.00180.2016.

[12] H. F. Posada-Quintero et al., "Time-varying analysis of electrodermal activity during exercise," PLoS ONE, vol. 13, no. 6, p. e0198328, Jun. 2018, doi: 10.1371/journal.pone.0198328.

[13] H. Wang, K. Siu, K. Ju, and K. H. Chon, "A High Resolution Approach to Estimating Time-Frequency Spectra and Their Amplitudes," Ann Biomed Eng, vol. 34, no. 2, pp. 326–338, Feb. 2006, doi: 10.1007/s10439-005-9035-y.

[14] V. Bisogni, M. F. Pengo, G. Maiolino, and G. P. Rossi, "The sympathetic nervous system and catecholamines metabolism in obstructive sleep apnoea," Journal of Thoracic Disease, vol. 8, no. 2, Feb. 2016, doi: 10.3978/j.issn.2072-1439.2015.11.14.

[15] H. U. Dissanayake et al., "Association between autonomic function and obstructive sleep apnea: A systematic review," Sleep Medicine Reviews, vol. 57, p. 101470, Jun. 2021, doi: 10.1016/j.smrv.2021.101470.

[16] E. I. Huang et al., "Respiratory Arousals in Patients with Very Severe Obstructive Sleep Apnea and How They Change after a Non-Framework Surgery," Healthcare (Basel), vol. 10, no. 5, p. 902, May 2022, doi: 10.3390/healthcare10050902.

[17] B. K. Lester, N. R. Burch, and R. C. Dossett, "NOCTURNAL EEG-GSR PROFILES: THE INFLUENCE OF PRESLEEP STATES," Psychophysiology, vol. 3, no. 3, pp. 238–248, Jan. 1967, doi: 10.1111/j.1469-8986.1967.tb02701.x.

[18] H. F. Posada-Quintero and K. H. Chon, "Innovations in Electrodermal Activity Data Collection and Signal Processing: A Systematic Review," Sensors, vol. 20, no. 2, p. 479, Jan. 2020.

[19] A. Azarbarzin, M. Ostrowski, P. Hanly, M. Younes, "Relationship between Arousal Intensity and Heart Rate Response to Arousal," Sleep, vol. 37, no. 4, pp. 645–653, Apr. 2014, doi: 10.5665/sleep.3560.

[20] R. B. Berry et al., "The AASM Manual for the Scoring of Sleep and Associated Events RULES, TERMINOLOGY AND TECHNICAL SPECIFICATIONS," 2017.

[21] V. K. Somerset , M. E. Dyken, A. L. Mark, and F. M. Abboud, "Sympathetic-Nerve Activity during Sleep in Normal Subjects," N Engl J Med, vol. 328, no. 5, pp. 303–307, Feb. 1993, doi: 10.1056/NEJM199302043280502

[22] K. Wang et al., "DREAMT: Dataset for Real-time sleep stage EstimAtion using Multisensor wearable Technology." PhysioNet, 2025, doi: 10.13026/0VRV-NN81.

[23] W. K. Wang et al., "Addressing wearable sleep tracking inequity: a new dataset and novel methods for a population with sleep disorders," in PMLR, 2024, pp. 380–396.

[24] A. L. Goldberger et al., "PhysioBank, PhysioToolkit, and PhysioNet: Components of a new research resource for complex physiologic signals," Circulation, vol. 101, no. 23, Jun. 2000, doi: 10.1161/01.cir.101.23.e215.

[25] I. Fernández-Varela et al., "A simple and robust method for the automatic scoring of EEG arousals in polysomnographic recordings," Computers in Biology and Medicine, vol. 87, pp. 77–86, Aug. 2017, doi: 10.1016/j.compbiomed.2017.05.011.

[26] D. Alvarez-Estevez and I. Fernández-Varela, "Large-scale validation of an automatic EEG arousal detection algorithm using different heterogeneous databases," Sleep Medicine, vol. 57, pp. 6–14, May 2019, doi: 10.1016/j.sleep.2019.01.025.

[27] I. R. Kleckner et al., "Simple, Transparent, and Flexible Automated Quality Assessment Procedures for Ambulatory Electrodermal Activity Data," IEEE Trans Biomed Eng, vol. 65, no. 7, pp. 1460–1467, Jul. 2018, doi: 10.1109/TBME.2017.2758643.

[28] M. de Zambotti, J. Trinder, A. Silvani, I. M. Colrain, and F. C. Baker, "Dynamic coupling between the central and autonomic nervous systems during sleep: A review," Neuroscience & Biobehavioral Reviews, vol. 90, pp. 84–103, Jul. 2018, doi: 10.1016/j.neubiorev.2018.03.027.